
AFRL-OSR-VA-TR-2014-0087

# (YIP-10) BIOTIC-ABIOTIC NANOSCALE INTERACTIONS IN BIOLOGICAL FUEL CELLS

**Mohamed El-Naggar**
**UNIVERSITY OF SOUTHERN CALIFORNIA LOS ANGELES**

**03/28/2014**
**Final Report**



Air Force Research Laboratory
AF Office Of Scientific Research (AFOSR)/ RTE
Arlington, Virginia 22203
Air Force Materiel Command

# REPORT DOCUMENTATION PAGE

*Form Approved*
*OMB No. 0704-0188*



| **1. REPORT DATE** *(DD-MM-YYYY)* | **2. REPORT TYPE** | **3. DATES COVERED** *(From - To)* |
|---|---|---|
| 03-24-2014 | final | 04/15/2010 - 12/31/2013 |

**4. TITLE AND SUBTITLE**

Biotic-Abiotic Nanoscale Interactions in Biological Fuel Cells

**5a. CONTRACT NUMBER**

**5b. GRANT NUMBER**
FA9550-10-1-0144

**5c. PROGRAM ELEMENT NUMBER**

**6. AUTHOR(S)**
Mohamed Y. El-Naggar

**5d. PROJECT NUMBER**

**5e. TASK NUMBER**

**5f. WORK UNIT NUMBER**

**7. PERFORMING ORGANIZATION NAME(S) AND ADDRESS(ES)**
University of Southern California
Prof. M.Y. El-Naggar, Seaver Science Center (SSC) 215C
920 Bloom Walk, Los Angeles, CA 90089-0484

**8. PERFORMING ORGANIZATION REPORT NUMBER**

**9. SPONSORING / MONITORING AGENCY NAME(S) AND ADDRESS(ES)**
Patrick O. Bradshaw, PhD
Program Manager
Air Force Office of Scientific Research
875 North Randolph Street 4027
Arlington VA 22203

**10. SPONSOR/MONITOR'S ACRONYM(S)**
AFOSR

**11. SPONSOR/MONITOR'S REPORT NUMBER(S)**

**12. DISTRIBUTION / AVAILABILITY STATEMENT**
Distribution A - Approved for Public Release

**13. SUPPLEMENTARY NOTES**

**14. ABSTRACT**

In contrast to metals and semiconductors, where the mechanisms of charge transfer are well understood, with immense technological consequences ranging from computers to solar cells, comparatively little is known about the physics of biological charge transfer, especially over long distances and at microbe-surface interfaces. Understanding this complex process will allow us to direct electronic signals from and to cells, potentially leading to new bioelectronics that combine the replication, self-repair, and precise biochemical control of nature with the vast toolbox of nanotechnology. This understanding will improve the flexibility and performance of future multifunctional DoD-relevant devices (energy harvesters, sensors, and bioelectronic circuits) that combine natural and synthetic components. In addition, the unique cell-to-surface conduits evolved by microbes are being exploited in diverse technologies ranging from bioremediation and biocorrosion control to microbial fuel cells. This AFOSR project has experimentally demonstrated micrometer scale electron transport along extracellular filaments known as bacterial nanowires, uncovered the underlying electron transport mechanisms, and developed in vivo techniques to study and harness this interfacial electron transport.

**15. SUBJECT TERMS**

| **16. SECURITY CLASSIFICATION OF:** | | | **17. LIMITATION OF ABSTRACT** | **18. NUMBER OF PAGES** | **19a. NAME OF RESPONSIBLE PERSON** |
|---|---|---|---|---|---|
| **a. REPORT** | **b. ABSTRACT** | **c. THIS PAGE** | UU | 6 | Mohamed Y. El-Naggar |
| U | U | U | | | **19b. TELEPHONE NUMBER** *(include area code)* 213-740-2394 |

# AFOSR Final Performance Report

**Project Title:** Biotic-Abiotic Nanoscale Interactions in Biological Fuel Cells

**Award Number:** FA9550-10-1-0144

**Start Date:** 04/15/2010

**Program Manager:**
Patrick O. Bradshaw, PhD
Air Force Office of Scientific Research
875 North Randolph Street 4027
Arlington VA 22203
email: Patrick.Bradshaw@afosr.af.mil
phone: 703-588-8492

**Principal Investigator:**
Mohamed Y. El-Naggar
Department of Physics and Astronomy
University of Southern California
920 Bloom Walk
Seaver Science Center 215C
Los Angeles, CA 90089-0484
email: mnaggar@usc.edu
phone: 213-740-2394

# Biotic-Abiotic Nanoscale Interactions in Biological Fuel Cells

## 1. Summary and Objectives

This research project, part of the Young Investigator Program (YIP), was motivated by the need to understand and control electron transport at the biotic-abiotic interface in microbial fuel cells (MFCs), where microbes are used as biocatalysts to oxidize organic fuels while routing the resulting electricity to anodes. Another impacted technology is the reverse process of microbial electrosynthesis, where renewable electrical energy (e.g. solar) drives reductive microbial metabolisms for synthesis of high value electrofuels. In particular, the project's primary objective was to elucidate the role of extracellular filaments known as bacterial nanowires. It was previously hypothesized that bacterial nanowires are electrically conductive and can mediate electron transport to fuel cell electrodes, but until our work there had been no direct measurements of micrometer-scale electrical transport to confirm this hypothesis. To accomplish this goal, we proposed to develop new approaches for interfacing bacterial nanowires from the model metal-reducer *Shewanella oneidensis* MR-1 to nanoscale electrodes, directly measure their conductance, and identify the physical mechanism of long-range charge transport. In addition, we proposed to study the extent to which this extracellular electron transport strategy is widespread in different microbial communities, and to develop new methods for monitoring bacterial nanowires and associated redox vesicles *in vivo*.

The above-mentioned objectives were met during the project's three-year timeline (see accomplishments below). As a result, we requested, and received, funds to extend the effort for one more year. Under the guidance of the program manager (Dr. Pat Bradshaw), we shifted our focus from the microbial fuel cell application to more generally explore bacterial nanowires for channeling electronic signals between synthetic devices and the electron transport chains of living cells. The extension objectives were (1) to directly wire bacterial cells (*S. oneidensis* MR-1) *in vivo* to micro/nano scale electrodes in microfluidic devices, and (2) to initiate a collaborative effort to profile the gene expression patterns underlying the display of bacterial nanowires, as the first step towards the future development of switches for controlling nanowire display.

## 2. Accomplishments and Highlights

**2.1** The first reported (and published) measurements of charge transfer along bacterial nanowires. The measured electron transfer rates allow for bacterial nanowires to serve as a viable microbial strategy for extracellular electron transport, with significant implications for biofuel cells.

**2.2** We identified the biophysical mechanism responsible for long-distance charge transport in *Shewanella* nanowires: multistep hopping in microbial redox chains. Mutants disrupted in specific multiheme cytochromes were found to be non-conductive, and our newly developed model of multistep electron hopping was found to be in agreement with both transverse and longitudinal conductance measurements in bacterial nanowires.

**2.3** Discovered and described a method for increasing microbial fuel cell power density using Ca ions as additives to encourage cellular aggregation – collaboration with Naval Research Lab.

**2.4** As part of an international collaboration, we reported on filamentous bacteria mediating centimeter-scale electron transport in marine sediments.

**2.5** Reported the first example of bacterial nanowires outside of environmental isolates, by measuring conductance in extracellular filaments from clinically relevant oral biofilms – collaboration with Ostrow School of Dentistry at USC.

**2.6** As part of an international collaboration, we discovered that transport in individual conductive bacterial nanowires can be controlled using an external gate voltage, demonstrating the first field-effect transistors based on bacterial nanowires.

**2.7** Developed a microfluidic platform for triggering and *in vivo* observations of bacterial nanowires. This platform provided the first direct (fluorescence) evidence of bacterial nanowire composition, and demonstrated the capability of directly wiring microbial cells to micro scale electrodes (Fig. 1).

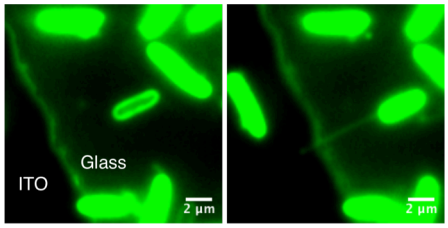


**Fig. 1.** Wiring *S. oneidensis* MR-1 cells to indium tin oxide (ITO) microelectrodes. Images before (left) and after (right) nanowire production triggered using the microfluidic platform developed during this project.

**2.8** Completed a time-dependent gene expression profiling (RNA-seq) study to elucidate the genetic mechanisms underlying nanowire production by *Shewanella oneidensis* MR-1 – collaboration with John Golbeck's group at Penn State.

**2.9** Developed an experimental platform combining optical trapping and microfluidic 3-electrode electrochemical chips to precisely manipulate live individual cells, place them on microscale 'landing pad' anodes, and detect the resulting cell-to-anode charge transfer. Preliminary testing resulted in single-cell measurements of cell-to-electrode electron transport. (Fig. 2). This platform, developed with AFOSR funding, is now being pursued for detailed mechanistic electron transport measurements with new DOE funding.

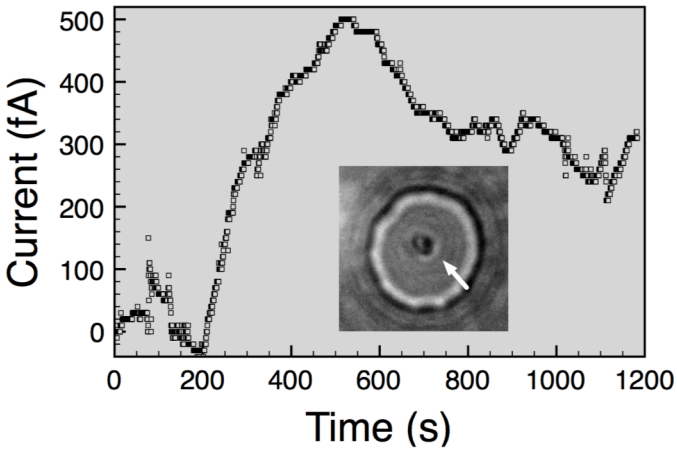


**Fig. 2.** Measurement of interfacial electron transfer (respiration current) from a single *Shewanella oneidensis* MR-1 cell (~300 fA). Arrow in inset points to a cell attached to the circular landing pad microscale anode.

Note: As of March 2014, accomplishments 2.1 – 2.6 have all been published (see publications below). Manuscripts corresponding to accomplishments 2.7 – 2.9 are either under review or in preparation.

## 3. Publications

### Published

K.M. Leung, G. Wanger, M.Y. El-Naggar, Y.A. Gorby, G. Southam, W.M. Lau, J. Yang. *Shewanella oneidensis MR-1 Bacterial Nanowires Exhibit p-Type, Tunable Electronic Behavior,* Nano Letters, 13(6), 2407-2411, 2013

G. Wanger, Y. Gorby, M.Y. El-Naggar, T.D. Yuzvinsky, C. Schaudinn, A. Gorur, P.P. Sedghizadeh. *Electrically conductive bacterial nanowires in bisphosphonate-related osteonecrosis of the jaw biofilms*, Oral Surgery, Oral Medicine, Oral Pathology and Oral Radiology, 115, 71-78, 2013

S. Pirbadian and M.Y. El-Naggar. *Multistep Hopping and Extracellular Charge Transfer in Microbial Redox Chains*, Physical Chemistry Chemical Physics, 14, 13802-13808, 2012.

C. Pfeffer, S. Larsen, J. Song, M. Dong, F. Besenbacher, R.L. Meyer, K. U. Kjeldsen, L. Schreiber, Y.A. Gorby, M. Y. El-Naggar, K. M. Leung, A. Schramm, N. Risgaard-Petersen and L. P. Nielsen. *Filamentous bacteria transport electrons over centimeter distances*, Nature, 419, 218-221, 2012.

L.A. Fitzgerald, E.R. Petersen, B.J. Gross, C.M. Soto, B.R. Ringeisen, M.Y. El-Naggar, and J.C. Biffinger. *Aggrandizing power output from Shewanella oneidensis MR-1 microbial fuel cells using calcium chloride*, Biosensors and Bioelectronics, 31 (1), 492-498, 2012

M.Y. El-Naggar, G. Wanger, K.M. Leung, T.D. Yuzvinsky, G.D. Southam, J. Yang, W.M. Lau, K.H. Nealson, and Y.A. Gorby. *Electrical transport along bacterial nanowires from Shewanella oneidensis MR-1*, Proceedings of the National Academy of Sciences of the Unites States of America, 107 (42), 18127-18131, 2010

### In Review

S. Pirbadian, S. E. Barchinger, K.M. Leung, H.S. Byun, Y. Jangir, R.A. Bouhenni, S.B. Reed, M.F. Romine, D.A. Saffarini, L. Shi, Y.A. Gorby, J. H. Golbeck, and M.Y. El-Naggar. *Shewanella oneidensis MR-1 bacterial nanowires are lipid-based extensions of the outer-membrane and periplasmic electron transport proteins*, Science Magazine, 2014

### In Preparation

B. Gross and M.Y. El-Naggar. *A combined optical trapping and bioelectrochemistry platform for single cell measurements of microbial respiration*, 2014

## 4. Interactions

### National Meetings, International Meetings, and Invited Seminars by M.Y. El-Naggar:

| | |
|---|---|
| 2009-2013 | Annual Air Force Office of Scientific Research Bioenergy Program Meeting, Arlington, VA |
| 2010 | American Chemical Society 241$^{st}$ National Meeting 'Microbial Fuel/Electrolysis Cells' Symposium (Keynote Speaker) |

| | |
|---|---|
| 2010 | Division of Engineering and Applied Science, California Institute of Technology, Pasadena, CA |
| 2011 | ASM International – Cal-State Northridge, Northridge, CA |
| 2011 | Department of Chemical Engineering and Materials Science, University of New Mexico, Albuquerque, NM. |
| 2011 | European Science Foundation Conference on Charge Transfer in Biosystems, Universitätszentrum Obergurgl, Austria |
| 2012 | Electrochemical Society 221st Meeting, Seattle, WA (Keynote Speaker) |
| 2012 | Berkeley Nanotechnology Forum, UC-Berkeley, CA (Invited Speaker) |
| 2012 | University of North Carolina-Chapel Hill and Duke University Solar Energy Research Center Meeting, Durham, NC (Invited Speaker) |
| 2013 | California State University – Los Angeles Department of Physics Colloquium |
| 2013 | University of Southern California Annual Trustees Meeting |
| 2013 | University of Southern California Molecular and Computational Biology Seminar |
| 2013 | Pacific Northwest National Lab '*Frontiers in Biological Sciences*' Seminar |
| 2013 | University of Minnesota Biotechnology Institute Seminar |
| 2013 | California State University, Long Beach Physics Colloquium |
| 2014 | Okayama University, Japan. Mini-Symposium on Biogenic and Multifunctional Materials |

## 5. Honors (M.Y. El-Naggar)

| | |
|---|---|
| 2010-2013 | Air Force Office of Scientific Research DoD Young Investigator Program Award |
| 2012 | Selected by *Popular Science* Magazine as one of the "Brilliant 10" of 2012 |
| 2013 | USC Dornsife Raubenheimer award for outstanding junior faculty member |
| 2013 | Presidential Early Career Award for Scientists and Engineers (PECASE) |

## 6. Trainees as part of this AFOSR project

**Postdoctoral Research Associates Supervised**

| | |
|---|---|
| 2009-2011 | Thomas Yuzvinsky, Ph.D. |
| 2011-2013 | Kar Man 'Edmond' Leung, Ph.D. |

**Graduate Students – USC Physics Ph.D. Program (Expected Graduation)**

| | |
|---|---|
| 2009-2013 | Benjamin J. Gross (2015) |
| 2011-2013 | Sahand Pirbadian (2016) |
| 2011-2012 | Yamini Jangir (2017) |
| 2012-2013 | Hye Suk Byun (2017) |

## 7. Conclusions

As a result of this work, we now know that microbes transport electrons along bacterial nanowires over much larger length scales than previously thought. In addition to pioneering the experimental measurement techniques used in this area, we developed theoretical models for long-range charge transfer via multistep hopping in biological redox chains, with implications for fundamental physiology and applied bioelectrochemistry (microbial fuel and electrosynthesis cells). Our work provides evidence that these biotic components can be used for channeling electronic signals between synthetic devices and the electron transport chains of live cells, potentially leading to new biosystems that combine the replication, self-repair, and precise biochemical control of nature with the vast toolbox of synthetic materials and nanotechnology. We are currently harnessing the understanding gained by this project's combined experimental/theoretical approach to characterize the interfacial metabolic and signaling events taking place between single cells and solid-state electrodes.

# Electrical transport along bacterial nanowires from *Shewanella oneidensis* MR-1

Mohamed Y. El-Naggar[a,1], Greg Wanger[b], Kar Man Leung[c,d], Thomas D. Yuzvinsky[a], Gordon Southam[e], Jun Yang[c], Woon Ming Lau[d], Kenneth H. Nealson[b,f], and Yuri A. Gorby[b]

[a]Department of Physics and Astronomy, [f]Departments of Earth Sciences and Biological Sciences, University of Southern California, Los Angeles, CA 90089; [b]The J. Craig Venter Institute, San Diego, CA 92121; [c]Department of Mechanical and Materials Engineering, University of Western Ontario, London, ON, Canada N6A 5B9; [d]Surface Science Western, University of Western Ontario, London, ON, Canada N6G 0J3; and [e]Department of Earth Sciences, University of Western Ontario, London, ON, Canada N6A 3K7

Edited by James M. Tiedje, Center for Microbial Ecology, East Lansing, MI, and approved August 31, 2010 (received for review April 9, 2010)

**Bacterial nanowires are extracellular appendages that have been suggested as pathways for electron transport in phylogenetically diverse microorganisms, including dissimilatory metal-reducing bacteria and photosynthetic cyanobacteria. However, there has been no evidence presented to demonstrate electron transport along the length of bacterial nanowires. Here we report electron transport measurements along individually addressed bacterial nanowires derived from electron-acceptor–limited cultures of the dissimilatory metal-reducing bacterium *Shewanella oneidensis* MR-1. Transport along the bacterial nanowires was independently evaluated by two techniques: (*i*) nanofabricated electrodes patterned on top of individual nanowires, and (*ii*) conducting probe atomic force microscopy at various points along a single nanowire bridging a metallic electrode and the conductive atomic force microscopy tip. The *S. oneidensis* MR-1 nanowires were found to be electrically conductive along micrometer-length scales with electron transport rates up to $10^9$/s at 100 mV of applied bias and a measured resistivity on the order of 1 Ω·cm. Mutants deficient in genes for *c*-type decaheme cytochromes MtrC and OmcA produce appendages that are morphologically consistent with bacterial nanowires, but were found to be nonconductive. The measurements reported here allow for bacterial nanowires to serve as a viable microbial strategy for extracellular electron transport.**

bioelectronics | microbial fuel cells | bioenergy

Electron transfer is fundamental to biology: organisms extract electrons from a wide array of electron sources (fuels) and transfer them to electron acceptors (oxidants). Prokaryotes can use a wide variety of dissolved electron acceptors (such as oxygen, nitrate, and sulfate) that are accessible to their intracellular enzymes. However, dissimilatory metal-reducing bacteria (DMRB) are challenged by the low solubility of solid phase Fe(III) and Mn(IV) minerals that serve as their terminal electron acceptors, and therefore use extracellular electron transfer to overcome this obstacle (1). Various strategies of extracellular electron transfer have been reported for metal-reducing bacteria, including naturally-occurring (2) and biogenic (3–5) soluble mediators that shuttle electrons from cells to acceptors, as well as direct transfer using multiheme cytochromes associated with the outer membrane (6). Recent reports have also suggested that extracellular electron transport may be facilitated by conductive filamentous extracellular appendages called bacterial nanowires (7–9). The first report found bacterial nanowires in the DMRB *Geobacter* (7). A subsequent scanning tunneling microscopy study (8) demonstrated transverse electrical conduction in nanowires from other microorganisms, including another metal reducer (*Shewanella oneidensis* MR-1), an oxygenic photosynthetic cyanobacterium (*Synechocystis* PCC6803), and a thermophilic fermentative bacterium (*Pelotomaculum thermopropionicum*), when cultivated under conditions of electron acceptor limitation.

To date, several biological assays have demonstrated results consistent with electron transport along bacterial nanowires, including measurements of improved electricity generation in microbial fuel cells and enhanced microbial reduction of solid-phase iron oxides (7, 8, 10). However, our direct knowledge of nanowire conductivity has been limited to local measurements of transport only across the thickness of the nanowires (7–9). Thus far, there has been no evidence presented to verify electron transport along the length of bacterial nanowires, which can extend many microns, well beyond a typical cell's length. Here we report electron transport measurements along individually addressed bacterial nanowires derived from electron-acceptor limited cultures of the DMRB *S. oneidensis* MR-1.

## Results

**Direct Transport Measurements Using Nanofabricated Electrodes.** To fabricate two-contact devices, chemically fixed samples from continuous cultures were deposited on $SiO_2$/Si substrates with prepatterned metallic contact pads. The substrates were subsequently dehydrated in ethanol, critical-point dried, and examined using a dual-column scanning electron/focused ion beam (FIB) microscope. Individual bacterial nanowires were located using secondary electron imaging and were then contacted by ion beam- or electron beam-induced deposition of platinum electrodes (Fig. 1). Current-voltage (I-V) sweeps were collected at ambient conditions using probe stations instrumented to semiconductor parameter analyzers.

Fig. 2 illustrates the results from a single bacterial nanowire extending from a wild-type *S. oneidensis* MR-1 cell. Following deposition of the Pt contacts (Fig. 2*A*), we observed an ohmic current response to applied voltage (Fig. 2*C*) with resistance $R$ = 386 MΩ, yielding a corresponding electron transport rate, at 100 mV, of about $10^9$ electrons per second. The resistivity estimated from this measurement is 1 Ω·cm (*Materials and Methods*), comparable in magnitude to that of moderately doped silicon nanowires (11). To confirm that the nanowire provides the only conductive path between the electrodes, a FIB was used to cut the nanowire without disturbing the rest of the device (Fig. 2*B*). After the nanowire was cut, there was no measurable current response to applied voltage (Fig. 2*C*), confirming that the observed conduction path was indeed through the nanowire. In addition to the nanowire of Fig. 2, two more bacterial nanowires, sampled from a different bioreactor, were investigated for electrical transport using nanofabricated electrodes, resulting in

Author contributions: M.Y.E.-N., K.M.L., G.S., J.Y., W.M.L., K.H.N., and Y.A.G. designed research; M.Y.E.-N., G.W., K.M.L., T.D.Y., and Y.A.G. performed research; M.Y.E.-N., G.W., K.M.L., T.D.Y., J.Y., W.M.L., K.H.N., and Y.A.G. analyzed data; and M.Y.E.-N., K.M.L., T.D.Y., and Y.A.G. wrote the paper.

The authors declare no conflict of interest.

This article is a PNAS Direct Submission.

[1]To whom correspondence should be addressed. E-mail: mnaggar@usc.edu.

This article contains supporting information online at www.pnas.org/lookup/suppl/doi:10.1073/pnas.1004880107/-/DCSupplemental.

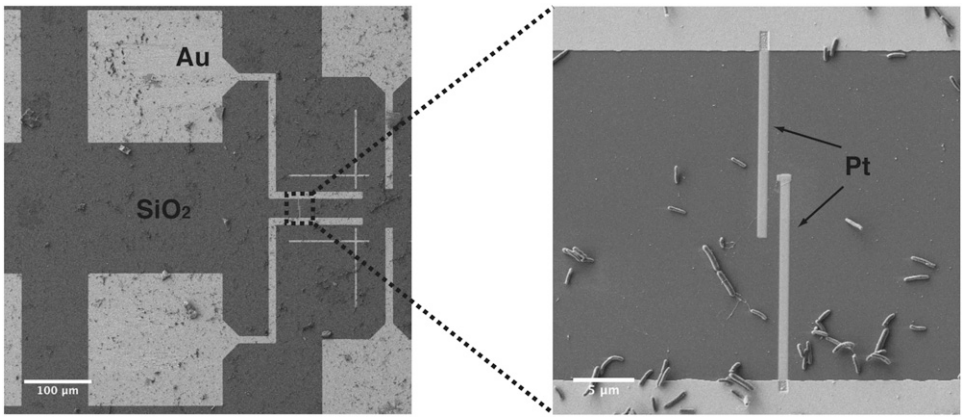


**Fig. 1.** Contacting individual bacterial nanowires with nanofabricated Pt electrodes. SEM images showing the geometry of the prefabricated Au contacts on $SiO_2$/Si. The zoom-in shows the FIB-deposited Pt contacts addressing a bacterial nanowire emanating from a *S. oneidensis* MR-1 cell.

measured resistivities of 4 Ω·cm ($R$ = 465 MΩ) (Fig. S1*A*) and 17 Ω·cm ($R$ = 2.3 GΩ) (Fig. S1*B*).

**Conducting Probe Atomic Force Microscopy.** To determine whether the resistivity values obtained from our two-contact devices include a significant contribution from contact resistance between electrodes and nanowires, conducting probe atomic force microscopy (CP-AFM) was used to measure the resistance of a single nanowire as a function of its length. CP-AFM is a convenient tool for probing local electrical properties at the nanometer scale, and has been increasingly used for the electrical characterization of biological molecules (12–14). CP-AFM was also previously employed to demonstrate transverse conduction through bacterial nanowires produced by *Geobacter sulfurreducens* (7) and *S. oneidensis* MR-1 (9). In the previous experiments, however, the nanowires were supported on conductive surfaces of highly ordered pyrolytic graphite, precluding measurements of their longitudinal conduction. To verify longitudinal transport along bacterial nanowires using CP-AFM, *S. oneidensis* MR-1 nanowires from chemically fixed samples were immobilized on $SiO_2$/Si substrates with lithographically patterned Au microgrids as electrodes (Fig. 3*A*).

Electronic transport along a nanowire in contact with the Au microgrid was measured by using the Pt-coated AFM tip as a second electrode. With the AFM tip at the position shown in Fig. 3*B*, ~600 nm away from the Au electrode and in contact with the nanowire, we obtained the I-V curve shown in Fig. 3*C*. The current response to the applied voltage was found to be approximately linear and consistent with the results obtained using nanofabricated Pt electrodes (Fig. 2). As a control, we observed that whenever the AFM tip was placed directly on the $SiO_2$ surface, we obtained a background current of ~10 pA (Fig. 3*C*, *Inset*), confirming that extraneous conduction through adsorbed water layers or other contaminants was negligible.

Fig. 3*D* shows multiple measurements on the same nanowire at different points along its length. We observed a linear relationship between measured resistance and length, allowing us to extrapolate the curve to zero length to estimate the overall contact resistance. We obtained a value of 58 MΩ that, when subtracted from the total resistance, yields a bulk resistivity for the nanowire on the order of 1 Ω·cm, in agreement with measurements using nanofabricated Pt electrodes (Fig. 2).

**Nonconductive Appendages Produced by *S. oneidensis* MR-1 Mutants Deficient in MtrC and OmcA.** We also studied mutants (ΔmtrC/omcA) lacking genes for multiheme *c*-type cytochromes MtrC and OmcA (8). The ΔmtrC/omcA mutants were cultivated in continuous flow bioreactors under identical conditions as wild-

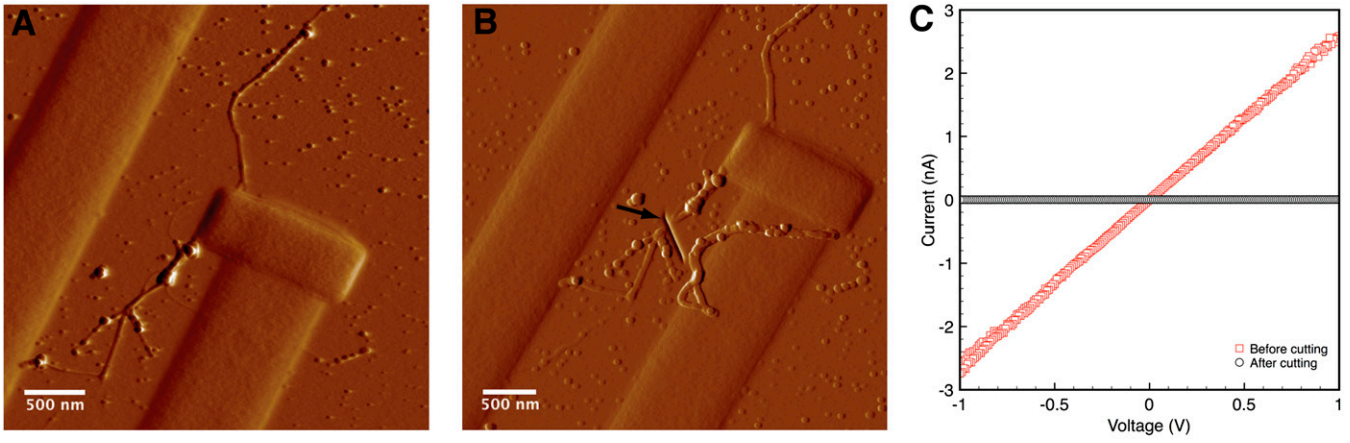


**Fig. 2.** Measuring electrical transport along a bacterial nanowire. (*A*) Tapping-mode atomic force microscopy (AFM) amplitude image detailing the contact area with the bacterial nanowire from Fig. 1. (*B*) Contact-mode AFM deflection image of the junction after cutting the nanowire with FIB milling. The arrow marks the cut location. (*C*) Current-voltage curve of the bacterial nanowire (ramp-up and ramp-down) both before (red) and after (black) cutting the nanowire.

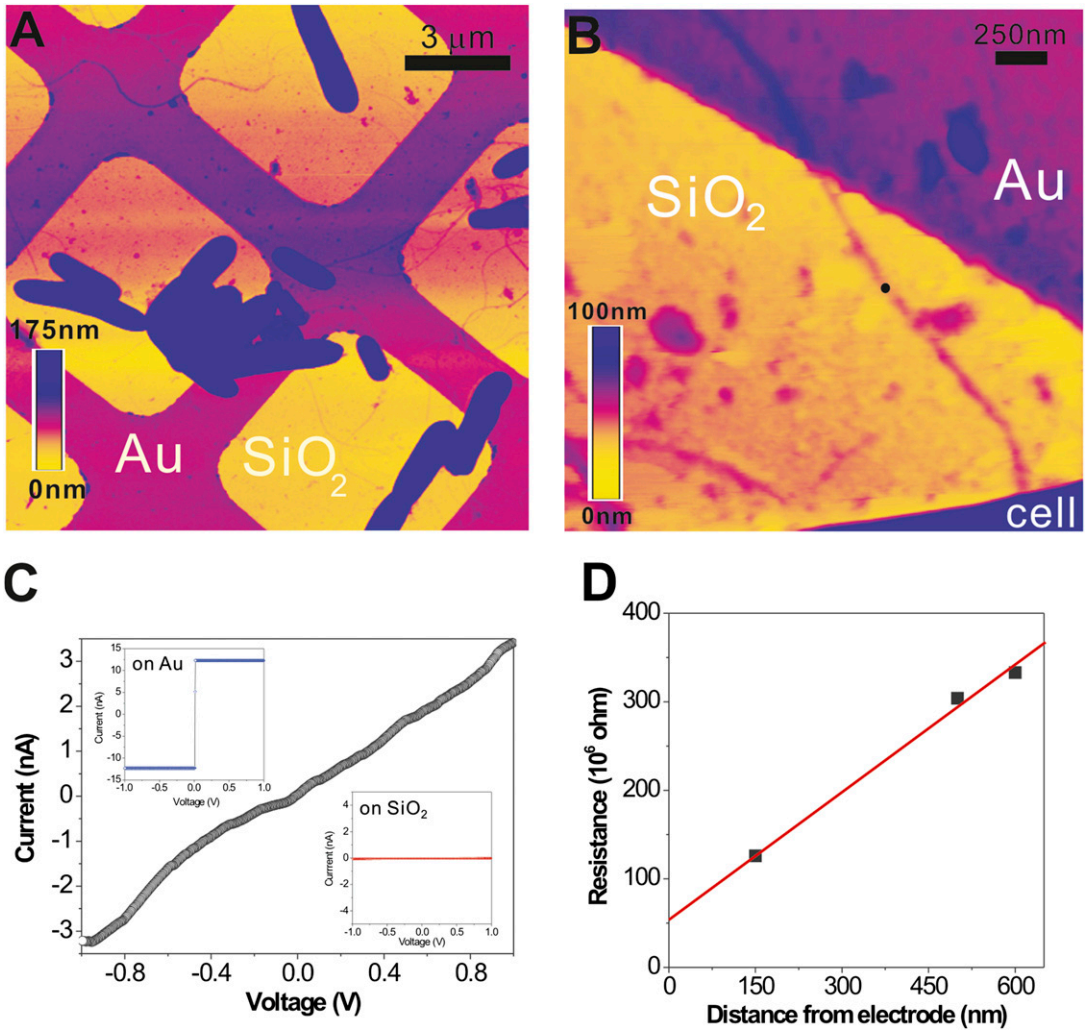


**Fig. 3.** CP-AFM of a bacterial nanowire. (*A*) Topographic AFM image showing air-dried *S. oneidensis* MR-1 cells and extracellular appendages deposited randomly on a $SiO_2$/Si substrate patterned with Au microgrids. (*B*) Contact mode AFM image showing a nanowire reaching out from a bacterial cell to the Au electrode. (*C*) An I-V curve obtained by probing the nanowire at a length of 600 nm away from the Au electrode (at the position marked by the black dot in *B*). (*Inset*) The I-V curves obtained on bare Au and $SiO_2$, respectively. (*D*) A plot of total resistance as a function of distance between AFM tip and Au electrode.

type MR-1. In response to electron acceptor limitation, the ΔmtrC/omcA mutants produced appendages morphologically consistent with wild-type nanowires (Fig. S2). A total of seven appendages, from seven different ΔmtrC/omcA cells and two bioreactor samples, were contacted by nanofabricated electrodes and tested for electrical conductivity (Fig. S2). The ΔmtrC/omcA appendages were found to be nonconductive, showing no current response to applied voltage down to the noise floor.

## Discussion

The discovery of bacterial nanowires spawned a common question among microbiologists, biogeochemists, and physicists: Can nanowires transport electrons along their entire length, and with what resistivity? To answer this question, we evaluated transport along bacterial nanowires by two independent techniques: (1) nanofabricated electrodes patterned on top of individual nanowires, and (2) CP-AFM at various points along a single nanowire bridging a metallic electrode and the conductive AFM tip. The *S. oneidensis* nanowires were found to be electrically conductive along micrometer-length scales with electron transport rates up to $10^9$/s at 100 mV of applied bias and a measured resistivity on the order of 1 Ω·cm.

Recent measurements by McLean et al. of the rate of electron transfer per cell from *S. oneidensis* MR-1 to fuel cell anodes were on the order of $10^6$ electrons per cell per second (15). These measurements are consistent with the specific respiration rate estimated under the cultivation conditions used here ($2.6 \times 10^6$ electrons per cell per second) (*Materials and Methods*). A comparison with our transport measurements demonstrates that a single bacterial nanowire could discharge this entire supply of respiratory electrons to a terminal acceptor.

A previous scanning tunneling microscopy study (8) associated *c*-type cytochromes with the conductivity of bacterial nanowires from *S. oneidensis* MR-1. To identify the role of cytochromes in nanowires, we studied mutants (ΔmtrC/omcA) lacking genes for multiheme *c*-type cytochromes MtrC and OmcA. We found that these mutants produce nonconductive filaments, indicating that, in the case of *S. oneidensis* MR-1, cytochromes are necessary for conduction along nanowires. However, this finding does not preclude other mechanisms for long-range electron transport along bacterial nanowires from other organisms. For example, *Geobacter* nanowires are presumed to be conductive as a result of the amino acid sequence of the type IV pilin subunit, PilA, and, possibly, the tertiary structure of the assembled pilus (7).

In conclusion, our data demonstrate electrical transport along bacterial nanowires from *S. oneidensis* MR-1, with transport rates that allow for bacterial nanowires to serve as a viable microbial strategy for extracellular electron transport. The measurements reported here motivate further investigations into the molecular composition and physical transport mechanism of bacterial nanowires, both to understand and realize the broad implications for natural microbial systems and biotechnological applications such as microbial fuel cells.

## Materials and Methods

**Cultivation.** *S. oneidensis* strain MR-1 (wild-type) and the double-deletion mutant ΔmtrC/omcA lacking two decaheme cytochromes were cultured in continuous flow bioreactors (BioFlo 110; New Brunswick Scientific) with a dilution rate of 0.05 $h^{-1}$ and an operating liquid volume of 1 L. A chemically defined medium was used with lactate as the sole electron donor, and conditions were maintained as previously described by Gorby et al. (8) to achieve electron acceptor limitation. Appendages were produced in response to electron acceptor ($O_2$) limitation, when the dissolved $O_2$ tension was lowered below the detection of the polarographic $O_2$ electrode.

An estimate of the specific respiration rate was calculated as follows: Starting with a wild-type *S. oneidensis* MR-1 bioreactor in steady state condition, cell density was determined using a Petroff-Hauser counting chamber to be $7.72 \times 10^8$ cells/mL. The flow of growth medium to the reactor was then shut off. Shortly thereafter, all the remaining electron donor (lactate) was consumed, triggering a rapid increase in dissolved $O_2$ concentration. Next, lactate was added to the reactor to a final concentration of 50 mM, with the oxidation of lactate immediately causing a rapid decrease in dissolved $O_2$ concentration. A subsequent rapid increase in dissolved $O_2$ concentration indicated that the lactate had been consumed. By measuring the time it took for the 50 mM lactate to be consumed (180 s), extracting 12 electrons per lactate molecule, and knowing the cell density, we calculate the rate of electron transfer per cell to be $2.6 \times 10^6$ electrons per cell per second.

**Nanofabricated Devices.** ***Sample preparation.*** Samples for electrical measurements using nanofabricated electrodes were removed from steady-state bioreactor cultures and immediately fixed using glutaraldehyde (2.5% concentration). Fixed samples were applied to oxidized Si chips with prepatterned Au contacts (Fig. 1) and subjected to a serial dehydration protocol using increasing concentrations of ethanol (10, 25, 50, 75, and finally 100% vol/vol ethanol). The dehydrated samples were then critical-point dried and desiccated for further nanofabrication processing.

***Electrode fabrication.*** Imaging and deposition were carried out using Zeiss 1540 XB FIB/SEM Etching/Deposition Systems. Cells with attached nanowires were located in the proximity of the prefabricated Au contacts. A Pt precursor was then introduced to the chamber using a gas injection system and electrodes were directly deposited to contact the bacterial nanowires using ion beam- (10 pA FIB current) or electron beam-induced chemical vapor deposition. The electrode sections in contact with the prefabricated Au contacts were always deposited by the FIB (which mills as it deposits), thus cleaning the prefabricated patterns of any cellular material that may have accumulated during sample preparation.

***Electrical measurements.*** Current-voltage (I-V) measurements were performed at room temperature using probe stations instrumented to either an Agilent 4156C semiconductor parameter analyzer or an Agilent B1500A analyzer. Results for three successful measurements of transport along bacterial nanowires from three different wild-type *S. oneidensis* MR-1 cells and two different samples are shown in Fig. 2 and Fig. S1. For each nanowire tested, resistance was calculated from the ohmic current-voltage (I-V) trace. Knowing the resistance ($R$, in Ω), the resistivity (ρ, in Ω·cm) was calculated using $\rho = \frac{RA}{L}$, where $L$ is the length of the nanowire segment between the two probes (measured by SEM or AFM imaging) and $A$ is the cross sectional nanowire area (calculated using AFM height measurements described below).

***Electrode characterization and controls.*** The Pt electrodes deposited by beam induced chemical vapor deposition were characterized separately to assess their contribution to the measured resistance. Fig. S3*A* shows a FIB-deposited Pt line (30-nm thick, 1-μm wide, 27-μm long) connecting the prefabricated Au patterns. From a current of 93.2 μA at 1V, the resistivity of the FIB-deposited Pt is calculated to be about $10^{-3}$ Ω·cm, including some contribution from the contact resistance between the Pt and prefabricated Au. This resistivity value is higher than the resistivity of bulk Pt, which is expected because of the carbon and gallium contamination inherent in the FIB deposition process, but is still a small contribution to the overall resistance of the junctions involving bacterial nanowires (>100 MΩ in Fig. 2 and Fig. S1). In addition to cutting a bacterial nanowire (Fig. 2), another open-circuit control was conducted (Fig. S3*B*) by placing two Pt probes very close together (<150 nm without a bridging nanowire) on a chip that underwent the same glutaraldehyde fixation, dehydration, and critical-drying protocol as the bacterial nanowire junctions. This sample also showed no current response to applied voltage, further ruling out any metallic contamination between the electrodes under the deposition conditions used in this study.

***AFM of nanofabricated devices.*** Following nanofabrication and electrical measurements, samples were inspected using a Veeco Innova AFM employing either tapping mode (Fig. 2*A*) or contact mode (Fig. 2*B*). The typical appendage height was found to be 8–10 nm (Fig. S4). A typical electrode thickness, for the deposition conditions used here, was 30–40 nm. Repeated AFM scanning after electrode deposition and successful I-V measurements but before cutting the nanowire of Fig. 2 displaced some extracellular debris close to the junction area (e.g., placing material near the right electrode in Fig. 2*B* compared with Fig. 2*A*), but the junction remained conductive.

**CP-AFM.** ***Sample preparation.*** Au microgrids were fabricated on a $SiO_2$/Si substrate by standard photolithographic patterning followed by electron-beam vapor deposition of 3 nm of Cr (as an adhesion layer) and 20 nm of Au. Samples were harvested from the bioreactor, fixed using 2.5% glutaraldehyde, and applied to the Au microgrid chips. These chips were air-dried (no dehydration or critical point drying) and washed with deionized water to remove salts in the culture medium.

***Conducting probe atomic force measurements.*** An Au microgrid (Fig. 3) was electrically connected to the sample stage of an AFM system (Veeco Dimension V) using silver paint. Pt/Cr coated Si AFM probes (BudgetSensors ContE) with a nominal spring constant of 0.2 N/m were used for both tapping and contact mode imaging. The current vs. voltage (I-V) curves of Fig. 3 were measured in point-spectroscopy mode with a typical gain setting of 1 V/nA. The loading force applied for electrical measurements (Fig. 3) was 4 nN, which we found to be the minimum force required to establish a stable short-circuiting contact between the conductive AFM tip and the Au electrode. In many cases, an imaging force of 10 nN or greater began to dislocate and damage the biological structures. Under such conditions, the apex of the conductive AFM tip could be coated with insulating debris. The minimum force (4 nN) was chosen for the electrical measurements to maintain an intimate electrical contact and not to damage the delicate nanowires. The sample voltage was ramped between −1 and 1 V at 0.2 Hz, yielding consistent and repeatable data. The resistance at each position along the nanowire was calculated using the most linear part (±0.4 V) of the I-V curve.

**ACKNOWLEDGMENTS.** We thank C. Zhou's research group and S. Cabrini for experimental help. Nanofabrication was conducted at the Lawrence Berkeley National Laboratory Molecular Foundry, University of California Riverside Center for Nanoscale Science and Engineering, and the Western Nanofabrication Laboratory. This work was supported by the Air Force Office of Scientific Research MURI FA9550-06-1-0292 and YIP FA9550-10-1-0144. Work at the Molecular Foundry was supported by the Office of Basic Energy Sciences of the US Department of Energy under Contract DE-AC02-05CH11231. This research was partially supported through a grant from the Legler-Benbough Foundation (San Diego, CA), internal funding from the J. Craig Venter Institute, and by the Canadian Natural Science and Engineering Research Council, Interdisciplinary Development Initiatives Program, Canada Foundation for Innovation, and Surface Science Western.

1. Chang IS, et al. (2006) Electrochemically active bacteria (EAB) and mediator-less microbial fuel cells. *J Microbiol Biotechnol* 16:163–177.
2. Lovley DR, Coates JD, Blunt-Harris EL, Phillips EJP, Woodward JC (1996) Humic substances as electron acceptors for microbial respiration. *Nature* 382:445–448.
3. Newman DK, Kolter R (2000) A role for excreted quinones in extracellular electron transfer. *Nature* 405:94–97.
4. Marsili E, et al. (2008) *Shewanella* secretes flavins that mediate extracellular electron transfer. *Proc Natl Acad Sci USA* 105:3968–3973.
5. von Canstein H, Ogawa J, Shimizu S, Lloyd JR (2008) Secretion of flavins by *Shewanella* species and their role in extracellular electron transfer. *Appl Environ Microbiol* 74: 615–623.
6. Myers CR, Myers JM (1992) Localization of cytochromes to the outer membrane of anaerobically grown *Shewanella* putrefaciens MR-1. *J Bacteriol* 174: 3429–3438.
7. Reguera G, et al. (2005) Extracellular electron transfer via microbial nanowires. *Nature* 435:1098–1101.

8. Gorby YA, et al. (2006) Electrically conductive bacterial nanowires produced by *Shewanella oneidensis* strain MR-1 and other microorganisms. *Proc Natl Acad Sci USA* 103:11358–11363.
9. El-Naggar MY, Gorby YA, Xia W, Nealson KH (2008) The molecular density of states in bacterial nanowires. *Biophys J* 95:L10–L12.
10. Reguera G, et al. (2006) Biofilm and nanowire production leads to increased current in *Geobacter sulfurreducens* fuel cells. *Appl Environ Microbiol* 72:7345–7348.
11. Yu JY, Chung SW, Heath JR (2000) Silicon nanowires: Preparation, device fabrication, and transport properties. *J Phys Chem B* 104:11864–11870.
12. Cohen H, Nogues C, Naaman R, Porath D (2005) Direct measurement of electrical transport through single DNA molecules of complex sequence. *Proc Natl Acad Sci USA* 102:11589–11593.
13. Andolfi L, Cannistraro S (2005) Conductive atomic force microscopy study of plastocyanin molecules adsorbed on gold electrode. *Surf Sci* 598:68–77.
14. Cai LT, Tabata H, Kawai T (2001) Probing electrical properties of oriented DNA by conducting atomic force microscopy. *Nanotechnology* 12:211–216.
15. McLean JS, et al. (2010) Quantification of electron transfer rates to a solid phase electron acceptor through the stages of biofilm formation from single cells to multicellular communities. *Environ Sci Technol* 44:2721–2727.

# Supporting Information

## El-Naggar et al. 10.1073/pnas.1004880107

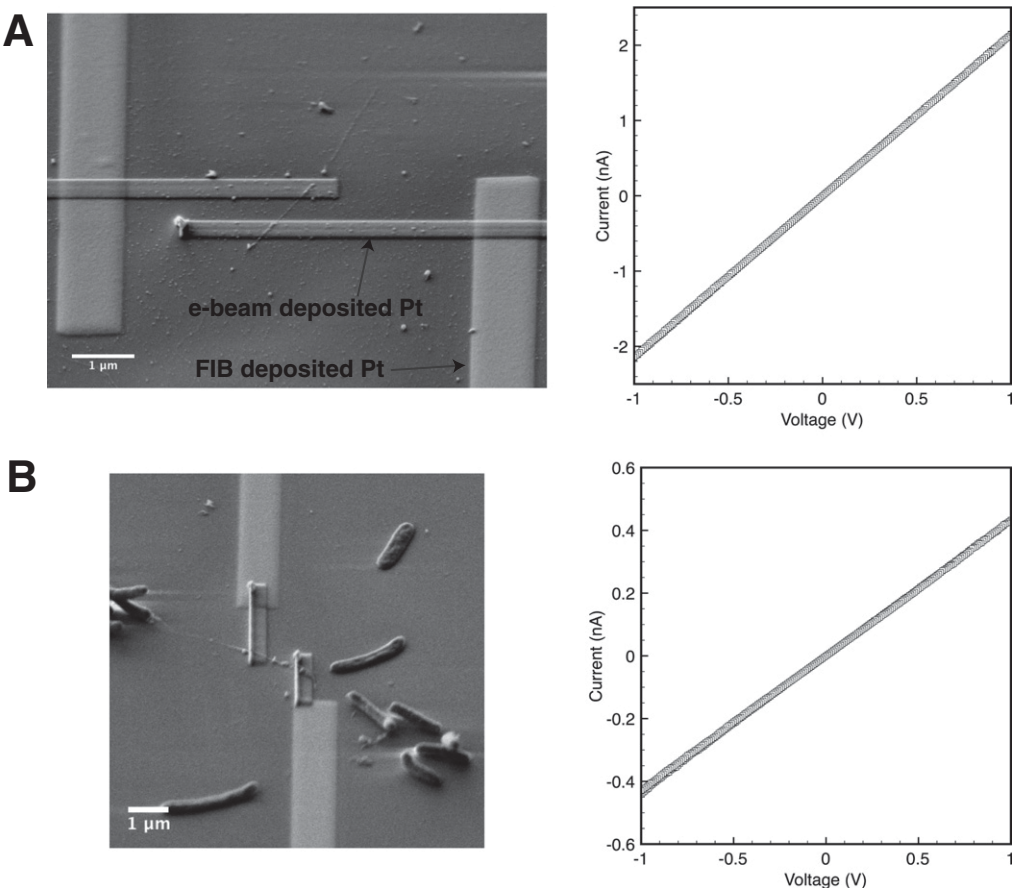


**Fig. S1.** Additional measurements of bacterial nanowires using nanofabricated electrodes. (*A*) SEM image of a bacterial nanowire addressed by a combination of focused ion beam (FIB) and e-beam deposited Pt contacts along with the current-voltage curve (ramp-up and down). (*B*) An additional bacterial nanowire (SEM) probed by a combination of FIB and e-beam deposited Pt electrodes and the associated current-voltage curve. SEM images in *A* and *B* are tilted by 54° to be at the coincidence point of the electron and FIBs.

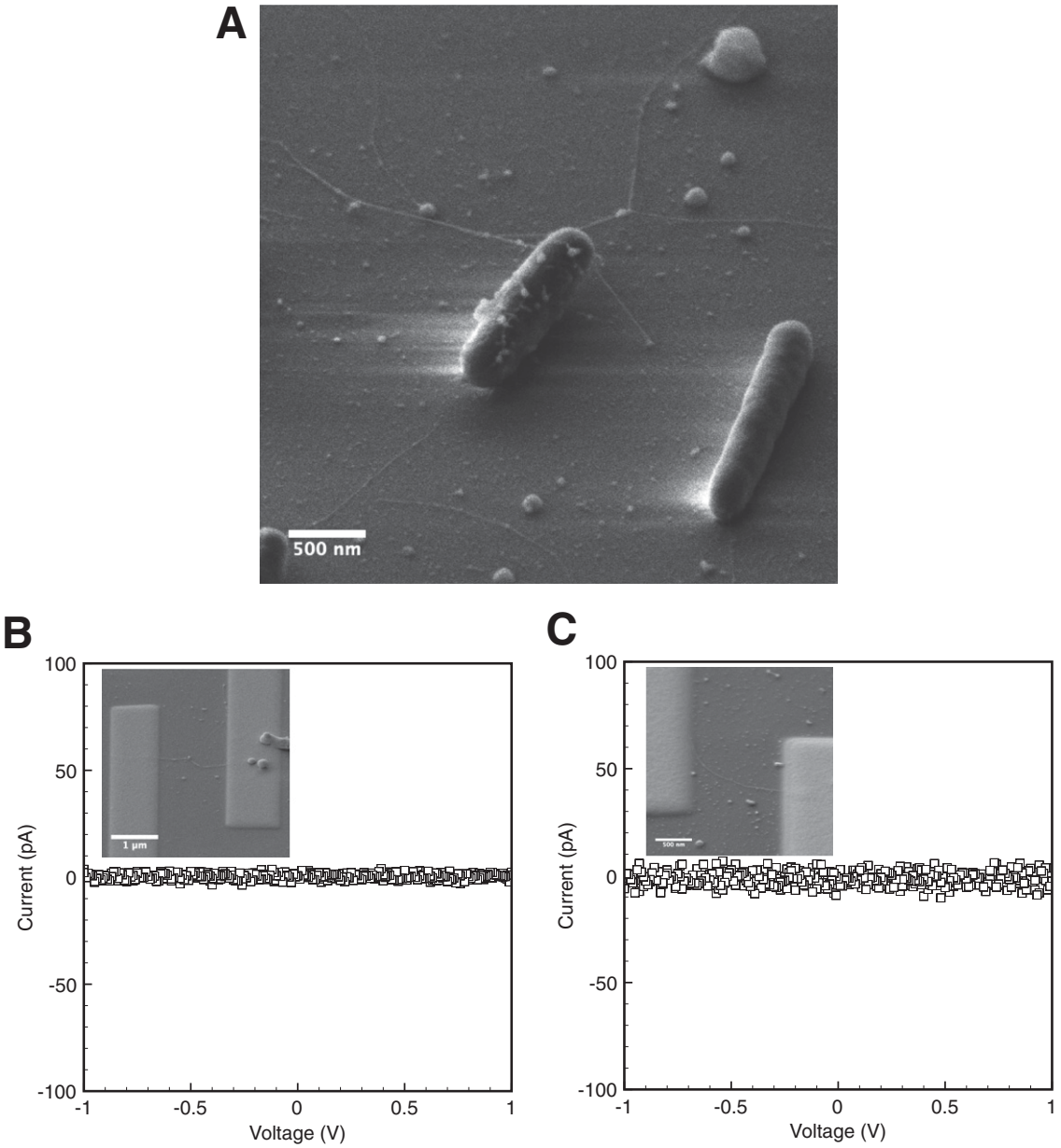


**Fig. S2.** Measurements of extracellular appendages from ΔmtrC/omcA mutants. (*A*) SEM image of a ΔmtrC/omcA mutant cell showing extracellular appendages morphologically consistent with bacterial nanowires. (*B* and *C*) I-V sweeps indicating two nonconductive appendages (SEM images in *Inset*) from ΔmtrC/omcA mutant cells (a total of seven mutant wires were tested, all nonconductive).

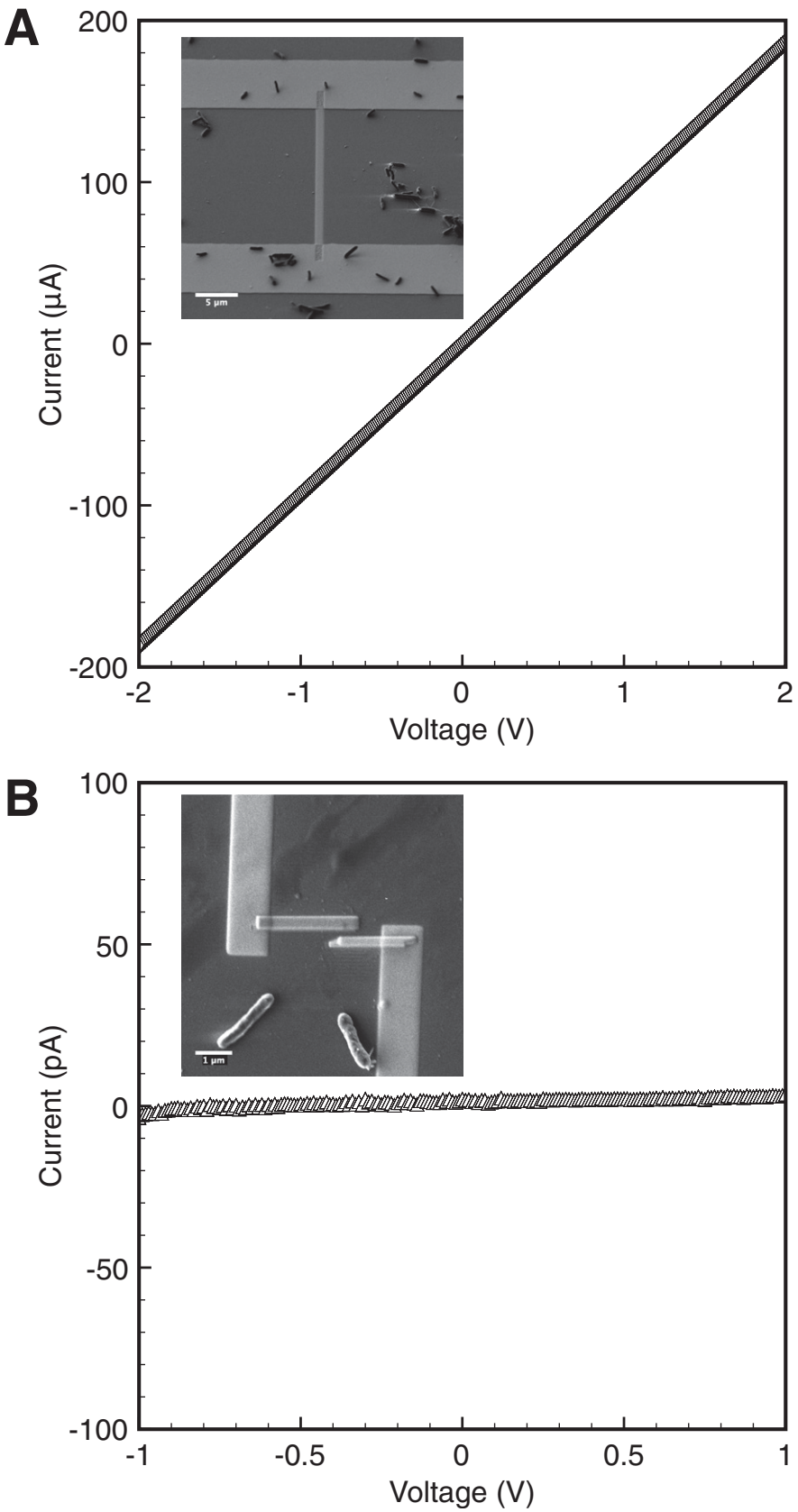


**Fig. S3.** Additional measurements and controls. (*A*) Characterizing a FIB-deposited Pt line resulting in the expected relatively low-resistance ohmic short-circuit behavior. (*B*) Open-circuit control resulting from 2 very closely spaced Pt electrodes on an $SiO_2$/Si chip undergoing the same fixation, dehydration, and critical point drying protocol, but with no nanowire bridging the gap.

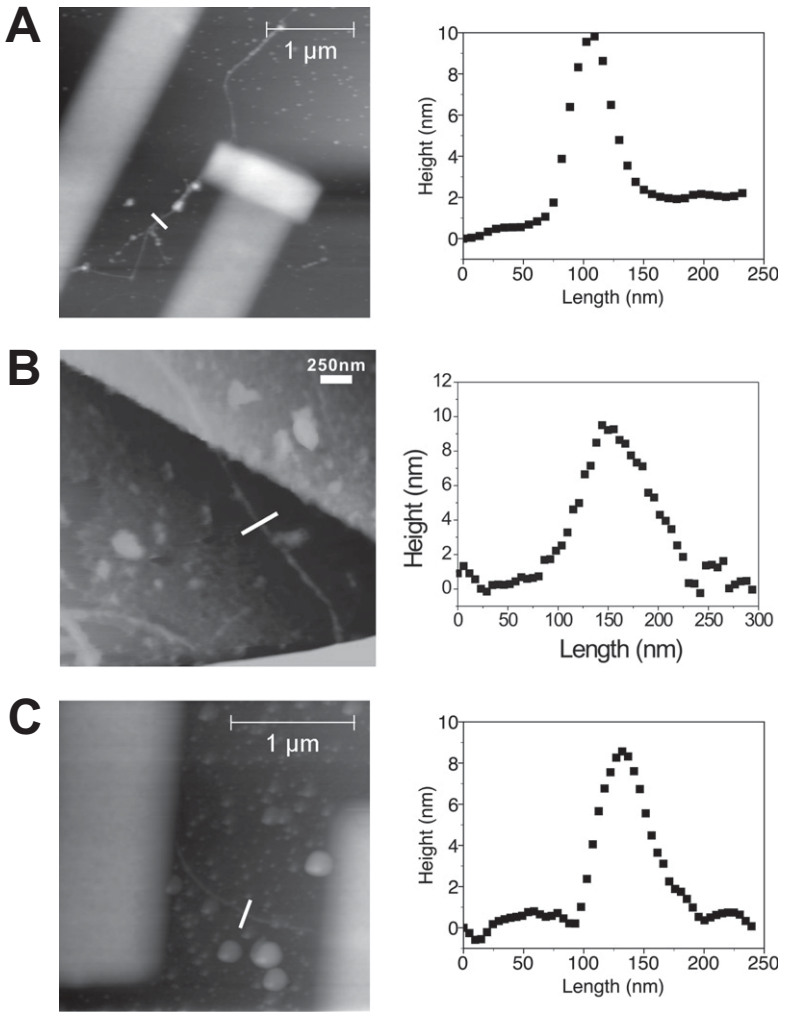


**Fig. S4.** AFM topography images and height profiles for the three types of samples analyzed in this study. (*A*) Bacterial nanowire from wild-type *S. oneidensis* MR-1 between two nanofabricated electrodes. (*B*) Bacterial nanowire from wild-type *S. oneidensis* MR-1 investigated using CP-AFM. (*C*) Nonconductive extracellular appendage from ΔmtrC/omcA between nanofabricated electrodes.

PCCP

Dynamic Article Links

Cite this: *Phys. Chem. Chem. Phys.*, 2012, **14**, 13802–13808

www.rsc.org/pccp

**PAPER**

# Multistep hopping and extracellular charge transfer in microbial redox chains†

**Sahand Pirbadian and Mohamed Y. El-Naggar***

***Received 12th April 2012, Accepted 18th June 2012***
**DOI: 10.1039/c2cp41185g**

Dissimilatory metal-reducing bacteria are microorganisms that gain energy by transferring respiratory electrons to extracellular solid-phase electron acceptors. In addition to its importance for physiology and natural environmental processes, this form of metabolism is being investigated for energy conversion and fuel production in bioelectrochemical systems, where microbes are used as biocatalysts at electrodes. One proposed strategy to accomplish this extracellular charge transfer involves forming a conductive pathway to electrodes by incorporating redox components on outer cell membranes and along extracellular appendages known as microbial nanowires within biofilms. To describe extracellular charge transfer in microbial redox chains, we employed a model based on incoherent hopping between sites in the chain and an interfacial treatment of electrochemical interactions with the surrounding electrodes. Based on this model, we calculated the current–voltage (*I–V*) characteristics and found the results to be in good agreement with *I–V* measurements across and along individual microbial nanowires produced by the bacterium *Shewanella oneidensis* MR-1. Based on our analysis, we propose that multistep hopping in redox chains constitutes a viable strategy for extracellular charge transfer in microbial biofilms.

## 1. Introduction

Electron transfer is a fundamental process in cellular respiration.[1,2] Organisms couple the oxidation of electron donors (*e.g.* organic matter, $H_2$, *etc.*) to the reduction of electron acceptors (oxidants). The flow of electrons, from donors to acceptors, is associated with the pumping of protons across a membrane to establish an electrochemical gradient that charges and energizes the cell, while driving the synthesis of biologically useful energy such as ATP. This strategy, called oxidative phosphorylation, is embraced by all respiratory microorganisms. Most eukaryotes and many prokaryotes are aerobic, using dissolved oxygen as a terminal electron acceptor for respiration. In addition, many anaerobic microbes are capable of reducing alternative dissolved acceptors, such as nitrates and sulfates. These dissolved acceptors react with donors through the electron transport chain *inside* living cells. The past two decades, however, have also brought about considerable interest in extracellular electron transfer (EET);[3,4] a respiratory strategy employed by microbes faced with the challenge of transferring electrons to terminal acceptors *outside* the cell itself. For example, dissimilatory metal-reducing bacteria (DMRB), including *Shewanella* and *Geobacter* spp, are known to gain energy by transferring respiratory electrons to minerals such as environmental Fe(III) and Mn(IV) oxides.[5,6]

*But how can a bacterium extend its electron transport chain to a solid outside the cell*? The answer to this fundamental question has important environmental and technological implications. Microbes performing EET are major players in biogeochemical cycles occurring at a global scale.[3] In addition, their unique metabolism has been exploited in diverse technologies ranging from bioremediation and biocorrosion control to energy harvesting in bioelectrochemical devices such as microbial fuel cells (MFCs).[7] In the latter, microbial biofilms are used as catalysts to oxidize diverse fuels and consequently perform EET to energy harvesting anodes, thus converting fuel to electricity.[8]

The strategies that DMRB are reported to employ for EET fall into two broad categories: indirect and direct mechanisms. Indirect mechanisms include naturally-occurring[9] or biogenic[10–12] soluble mediators that diffusively shuttle electrons from cells to solid external acceptors such as minerals or anodes. Direct mechanisms take advantage of cell-surface contact, using redox molecules such as multiheme *c* cytochromes located on the cell exterior[13,14] or by directing long-range transfer *via* conductive proteinaceous filaments known as microbial (or bacterial) nanowires.[15–19] It is important to note that

*Department of Physics and Astronomy, University of Southern California, 920 Bloom Walk, Seaver Science Center 215C, Los Angeles, CA 90089-0484, USA. E-mail: mnaggar@usc.edu; Fax: +1 213 740-6653; Tel: +1 213 740-2394*

† Electronic supplementary information (ESI) available: The sensitivity of the calculations to changes in the reorganization energy and the effective heterogeneous electron transfer rate constant. Table of calculation parameters used to model the transverse and longitudinal measurements. See DOI: 10.1039/c2cp41185g

organisms may switch between indirect and direct EET strategies depending on a number of factors, ranging from cultivation details to natural environmental conditions.[20] *Shewanella oneidensis* MR-1, for instance, has been shown to secrete flavins as soluble redox shuttles for EET.[11] At the same time, the genome of this organism encodes 42 different *c* cytochromes, some of which can be localized to the cell exterior and are known to be critical for direct EET to minerals and fuel cell anodes.[21] Furthermore, under conditions of electron acceptor limitation, *S. oneidensis* MR-1 can produce conductive microbial nanowires with electron transport rates up to $10^9$ $s^{-1}$ at 100 mV of applied bias and a measured resistivity on the order of 1 Ω cm; sufficient to keep up with the typical specific respiration rates of these microbes.[18] At the same time, mutants lacking specific multiheme cytochromes (MtrC and OmcA) produce non-conductive filaments under identical conditions, suggesting that extracellular redox sites are necessary for long-range EET *via* microbial nanowires.[18]

The present study focuses on the theoretical basis of how biotic components such as microbial nanowires and associated multiheme *c* cytochromes form conductive biofilms facilitating direct microbe-to-electrode EET. We build on two recent theoretical studies proposing multistep hopping in redox chains as the physical mechanism of this long-range charge transfer in *Geobacter* biofilms and *Shewanella* nanowires.[22,23] The proposed model is based on an incoherent multistep hopping mechanism between redox sites, and an interfacial treatment of non-adiabatic (Marcus theory) electron transfer rate equations to account for the electrochemical interactions with measurement electrodes.[24] Using this model, we compute current–voltage (*I–V*) curves consistent with both transverse and longitudinal experimental measurements of *Shewanella* nanowires (published data[17,18] and new higher-bias data reported here) as well as inter-site spacings from the recently determined crystal structure of *Shewanella* cytochromes.[25]

## 2. Modeling

### 2.1 Background

Previous charge transport measurements in microbial nanowires and biofilms were performed over length scales far exceeding the size of individual cells (>1 μm),[18,19,22] and are therefore beyond the scope of direct single-step tunneling mechanisms relevant over much shorter distances (<2 nm).[26] For this reason, the direct EET systems have been interpreted in light of two mechanisms: (i) fully coherent band conduction much like metals and semiconductors,[19] and (ii) incoherent multistep hopping between charge localizing sites, such as redox cofactors.[22,23] We start by considering the length and time scales involved in these physically distinct ideas, and consequently their applicability to microbial EET.

As discussed by Polizzi *et al.*,[23] band conduction requires that the scattering time of the carriers, $T_s$, and the width of the energy band, $W$, satisfy the condition $T_s W \gg \hbar$ with $\hbar$ being the Planck constant. The width of the energy band can be defined as $W = 4|H_{DA}|$, where $|H_{DA}|$ is the charge transfer integral between the localizing sites in the system. At the same time, the charge mobility in band theory is $\mu_{BT} = 2er^2|H_{DA}|T_s/\hbar^2$, where $e$ is the charge and $r$ is the distance between localizing sites.[27] Combining these expressions results in a fundamental requirement that $\mu_{BT} \gg er^2/2\hbar$. In other words, there is a minimum mobility for the band theory picture. Even using a small separation between neighboring sites, 0.35 nm (consistent with π-stacking in conducting polymers), this requires that the mobility be far greater than $\sim 1$ $cm^2$ $V$ $s^{-1}$.[23] However, from our previous measurements of *Shewanella* nanowires,[18] the conductivity is measured to be 1 S $cm^{-1}$ and the mobility can be estimated to be lower than $10^{-3}$ $cm^2$ $V$ $s^{-1}$.[23] While enough to sustain microbial respiration,[18] this is clearly well below the band theory limit. For this reason, we contend that fully coherent band conduction is not a viable model for microbial nanowire conductivity and therefore exclude the band picture in the model and experimental measurements described below. Other aspects of the applicability of band theory to describe previously reported experimental measurements in *Geobacter* nanowires[19] (also with mobilities far below the band limit described above) have been debated elsewhere.[28]

In the hopping picture, for an electron hopping process between two wells, the vibrational relaxation rate should be larger than the hopping rate for the hopping step to be independent of the preceding and succeeding hopping, *i.e.* $k_{rel} \gg k_{hop}$. This has recently been interpreted by Troisi[29] as a 'speed limit', imposing a maximum charge mobility for sequential hopping. Furthermore, this limit can be conveniently estimated from spectroscopic measurements in organic solids since the vibrational relaxation rate is given by $k_{rel} = 2\pi c\bar{\delta}$, where $c$ is the speed of light and $\bar{\delta}$ is the Raman line broadening.[29,30] Using standard values for molecular materials, $k_{rel}$ typically exceeds $10^{11}$ $s^{-1}$.[29] On the other hand $k_{hop}$ can be estimated from the non-adiabatic rate equation for electron transfer between two sites:[31]

$$k_{hop} = \frac{2\pi}{\hbar}\frac{|H_{DA}|^2}{\sqrt{4\pi\lambda k_B T}}\exp\left[-\frac{(\Delta G+\lambda)^2}{4\lambda k_B T}\right] \qquad (1)$$

where $\lambda$ is the reorganization energy of the system, $k_B$ is the Boltzmann constant, $T$ is the temperature, and $\Delta G$ is the free energy change as a result of the electron transfer. This expression is frequently encountered in the simplified phenomenological form:[23]

$$k_{hop}(s^{-1}) = 10^{13}\exp\left[-\beta R - \frac{(\Delta G+\lambda)^2}{4\lambda k_B T}\right] \qquad (2)$$

where $\beta$ is the tunneling decay factor ($\sim 1$ $Å^{-1}$), and $R$ is the effective tunneling distance between two neighboring sites (the difference between the nearest neighbor hopping distance and the distance at van der Waals contact, the latter taken to be 0.35 nm). At the maximum hopping rate for efficient biological electron transfer, $\lambda = -\Delta G$, and taking $R = 0.65$ nm, a value consistent with typical inter-cofactor distances in a *Shewanella* multiheme cytochrome,[25] this results in $k_{hop} = 1.5 \times 10^{10}$ $s^{-1}$. In summary, this rate can fall below the relaxation rate, allowing for independent hopping steps from electrode to electrode through a chain of redox sites.

### 2.2 Multistep hopping

The multistep hopping chain model is schematically illustrated in Fig. 1a, where $L$ redox sites bridge two measurement electrodes.

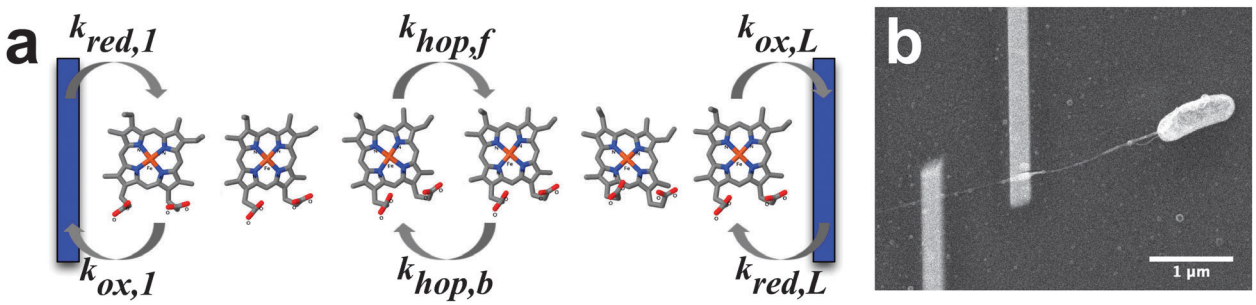


**Fig. 1** (a) A redox chain bridging two measurement electrodes. Forward and backward charge transfer rates within the redox chain are determined by $k_{hop,f}$ and $k_{hop,b}$ respectively, while the interactions with electrodes are determined by the electrochemical transfer rates $k_{red}$ and $k_{ox}$ at the left and right contacts. The redox sites pictured in the schematic represent hemes such as those found in the multiheme cytochromes of the dissimilatory metal-reducing bacterium *Shewanella oneidensis* MR-1. (b) Scanning electron microscopy image of an experimental platform, where two Pt electrodes address an individual microbial nanowire from a single *S. oneidensis* MR-1 cell (rod shaped cell to the right).

This picture is motivated by the experimental approaches recently used to measure the current response of one-dimensional structures such as microbial nanowires when a voltage $V$ is applied between the electrodes (Fig. 1b). The forward and backward electron transfer rates between redox sites within the chain are given by $k_{hop,f}$ and $k_{hop,b}$, both of which follow the expression for $k_{hop}$ above but with the corresponding $\Delta G$ values of $-eV/L$ and $eV/L$, respectively. This electron hopping step between sites $i$ and $i+1$ ($1 \le i \le L-1$) is represented by the following reaction:[22,29]

$$(i)_{reduced} + (i+1)_{oxidized} \underset{k_{hop,b}}{\overset{k_{hop,f}}{\rightleftharpoons}} (i)_{oxidized} + (i+1)_{reduced} \quad (3)$$

which in turns gives the electron flux between two neighboring redox sites as:[22]

$$J = k_{hop,f}P(i)[1 - P(i+1)] - k_{hop,b}P(i+1)[1 - P(i)] \quad (4)$$

where $P(i)$ denotes the occupation probability of site $i$ (reduced probability) and $1 - P(i)$ denotes the vacation probability of site $i$ (oxidized probability).

The heterogeneous transfer from/to the electrodes (electrochemical oxidation and reduction of the first or $L$'th site) is determined using the electrochemical form of the non-adiabatic electron transfer rate equation,[24] by considering the overlap between the electronic density of states in the metallic electrode, $\rho$ (Fermi–Dirac distribution), and the Gaussian oxidation or reduction peaks of the neighboring redox site, situated $+\lambda$ and $-\lambda$ with respect to the redox potential, as illustrated in Fig. 2. The rates $k_{red,\eta}$ and $k_{ox,\eta}$, representing electron transfer from and to an electrode (to and from site $\eta$ where $\eta = 1$ or $L$), are given by:[23,24]

$$k_{red,\eta} = C_{electrode} \int_{-\infty}^{\infty} \frac{\exp\left[-\left(x - \frac{\lambda + e(E-E^o)_\eta}{k_B T}\right)^2 \left(\frac{k_B T}{4\lambda}\right)\right]}{1+\exp(x)} dx \quad (5)$$

$$k_{ox,\eta} = C_{electrode} \int_{-\infty}^{\infty} \frac{\exp\left[-\left(x - \frac{\lambda - e(E-E^o)_\eta}{k_B T}\right)^2 \left(\frac{k_B T}{4\lambda}\right)\right]}{1+\exp(x)} dx \quad (6)$$

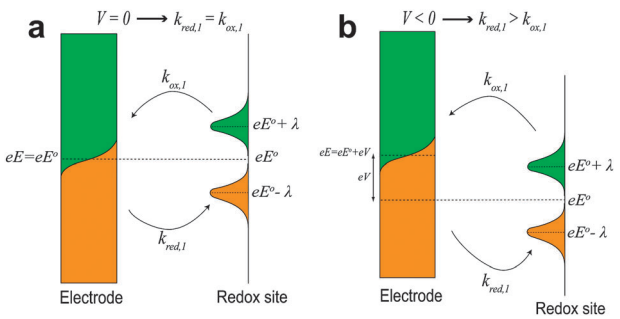


**Fig. 2** A schematic of the electrochemical interaction between the redox species and a neighboring electrode. Applying a voltage $V$ changes the relation of the metallic states with respect to the oxidation–reduction probability peaks of the redox site. (a) When $V = 0$, the Fermi energy of the metal electrode ($eE$) is equivalent to the redox energy ($eE^o$), leading the oxidation and reduction rates to balance, and therefore the net charge transfer is zero. (b) Applying a voltage shifts the energy level of the electrode with respect to the redox level, favoring reduction or oxidation ($V < 0$ pictured, leading to increased reduction rate).

where $C_{electrode} = \frac{2\pi}{\hbar}\sqrt{\frac{k_B T}{4\pi\lambda}}\overline{|H|^2}\rho$ and $(E - E^o)_\eta$ is the difference between the applied electrode potential ($E$) and the potential of its neighboring redox site ($E^o$) at either the left or right contact. The latter can also be represented as a local voltage drop. For example, at the left electrode, $(E - E^o)_1 = \alpha V$ where $\alpha$ is a fraction of the overall applied voltage $V$ between the two electrodes. These heterogeneous transfer rates allow the calculation of the charge flux at the left and right electrodes:[32]

$$J_1 = k_{red,1}[1 - P(1)] - k_{ox,1}P(1) \quad (7)$$

$$J_L = k_{ox,L}P(L) - k_{red,L}[1 - P(L)] \quad (8)$$

Two symmetric contact electrodes will lead to the same magnitude of local voltage drop at opposite electrodes, *i.e.* $(E - E^o)_1 = -(E - E^o)_L$, which in turn translates to $k_{red,1} = k_{ox,L}$ and $k_{ox,1} = k_{red,L}$. In addition, realizing that the charge flux from one electrode to the other is equal:

$$J_1 = k_{red,1}[1 - P(1)] - k_{ox,1}P(1) = J_L = k_{red,1}P(L) - k_{ox,1}[1 - P(L)] \Rightarrow P(L) = 1 - P(1) \quad (9)$$

Finally, realizing that the flux within the chain is equivalent to the flux at the electrodes, $J = J_1 = J_L$, combining eqn (4) and (9) gives the occupation probability throughout the chain as:

$$P(i+1) = \frac{k_{\mathrm{hop,f}}P(i) + k_{\mathrm{ox},1}P(1) - k_{\mathrm{red},1}[1 - P(1)]}{k_{\mathrm{hop,b}} + (k_{\mathrm{hop,f}} - k_{\mathrm{hop,b}})P(i)}; \quad 1 \le i \le L - 1, \tag{10}$$

Next, we apply this analysis to calculate the probability profiles and corresponding current–voltage ($I$–$V$) curves to compare with transverse and longitudinal transport measurements of microbial nanowires from the bacterium *S. oneidensis* MR-1.

## 3. Results and comparison to experiments

For a specific $V$ (applied bias), $L$ (number of sites), $R$ (effective tunneling distance), $\lambda$ (reorganization energy), $\alpha$ (fraction defining the contact voltage drop), $C_{\mathrm{electrode}}$ (pre-exponential of the heterogeneous transfer rates $k_{\mathrm{red}}$ and $k_{\mathrm{ox}}$), and $k_{\mathrm{B}}T$ (thermal energy), the model outlined above allows the calculation of the occupation probability profile throughout the redox chain, and consequently the overall current response to applied voltage. At each voltage step, the last site's occupation probability $P(L)$ can be calculated as a function of the first site's occupation probability $P(1)$, by solving eqn (10) recursively. Combining this relation with the symmetric constraint from eqn (9) results in a unique value for $P(1)$, which is dependent on the transfer rates $k_{\mathrm{hop,f}}$, $k_{\mathrm{hop,b}}$, $k_{\mathrm{ox}}$, and $k_{\mathrm{red}}$ (note all these rates are functions of voltage). Next, the entire probability profile $P(i)$ can be calculated from eqn (10). We performed this calculation in MATLAB, using parameters consistent with existing transverse (small $L$) and longitudinal (large $L$) $I$–$V$ measurements of *Shewanella* nanowires. The results described here assume the value of $k_{\mathrm{B}}T$ at room temperature, and take 1 nm as the typical distance between the redox sites (*i.e.* $R = 0.65$ nm), consistent with the recently measured inter-heme spacings in MtrF, a multiheme cytochrome from *Shewanella*.[25] We obtained excellent fits to the experimental data by assuming an effective heterogeneous transfer rate $C_{\mathrm{electrode}}$ smaller than the hopping rate between sites $k_{\mathrm{hop}}$. For each experiment, we calculate the probability profile and the conventional (positive) current ($I = -J$) as a function of applied bias $V$. Finally, we fit our calculations to $I$–$V$ measurements, and comment on the parameters $\lambda$, $\alpha$, and $C_{\mathrm{electrode}}$ that give rise to good agreement with these experiments.

Fig. 3 shows the calculated probability profile for a redox chain consisting of 2000 sites as the voltage is swept from 0 to 1 V. As the voltage increases the occupation probability rapidly changes from a linear and relatively flat profile to a sharp sigmoid with high occupation probability near one electrode and a high vacation probability near the opposing electrode. With the probability profile in hand, the corresponding $I$–$V$ behavior is simply calculated from $I = -J_1 = k_{\mathrm{ox},1}P(1) - k_{\mathrm{red},1}[1 - P(1)]$, and the result is plotted in Fig. 4. When $C_{\mathrm{electrode}} \ll k_{\mathrm{hop}}$, $P(1) \approx 1$ under positive bias, except near zero applied voltage (and similarly $P(1) \approx 0$ for negative non-small bias). Under these conditions, the current

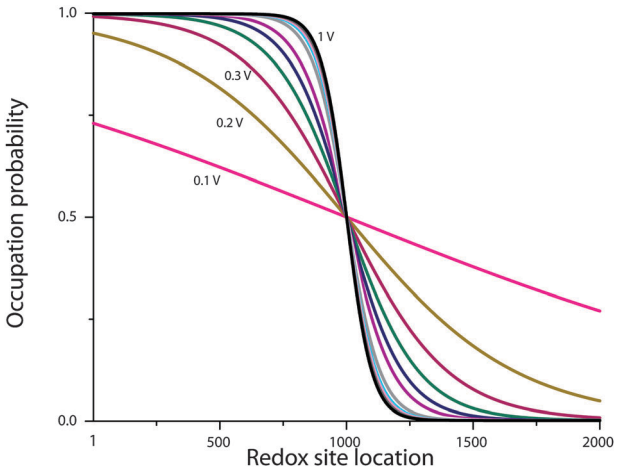


**Fig. 3** The occupation probability profile for a chain composed of $L = 2000$ redox sites as the applied voltage between the surrounding electrodes is stepped up in 0.1 V increments (corresponding to the experiment in El-Naggar *et al.*[18] and the calculated $I$–$V$ profiles of Fig. 4 and 5b). Calculation parameters: $L = 2000$, $\lambda = 0.4$ eV, $\alpha = 0.015$, $R = 0.65$ nm, $\beta = 1$ Å$^{-1}$, $k_{\mathrm{B}}T = 0.025$ eV.

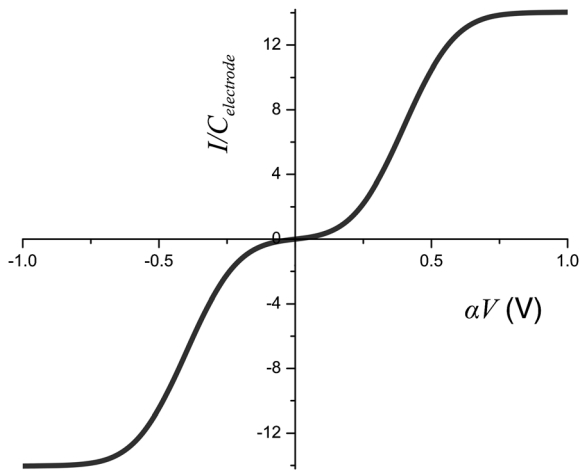


**Fig. 4** Calculated current as a function of the local electrode voltage drop for the $L = 2000$ redox chain (using eqn (7) and the occupation probability profile of Fig. 3). The current reaches a constant value when the overlap between the electrode's Fermi function and the redox peaks saturates at high applied voltage. Calculation parameters: $L = 2000$, $\lambda = 0.4$ eV, $\alpha = 0.015$, $R = 0.65$ nm, $\beta = 1$ Å$^{-1}$, $k_{\mathrm{B}}T = 0.025$ eV.

essentially follows the form of the heterogeneous electron transfer terms eqn (5) and (6) *i.e.* increasing the voltage increases the current response, until the overlap between the electrode's Fermi function and the Gaussian redox peaks saturates for very high voltages, as schematically illustrated in Fig. 2 and discussed elsewhere.[23]

We now compare the predictions of this model to measurements of transport in conductive microbial appendages, performed using two different experimental techniques. In the first experiment[17] (Fig. 5a) transverse transport is measured across the width (10 nm, corresponding to $L = 10$ in the model) of a microbial nanowire using a conductive atomic force microscope (c-AFM) tip as a top electrode and the underlying substrate as a bottom electrode. In the second experiment,[18]

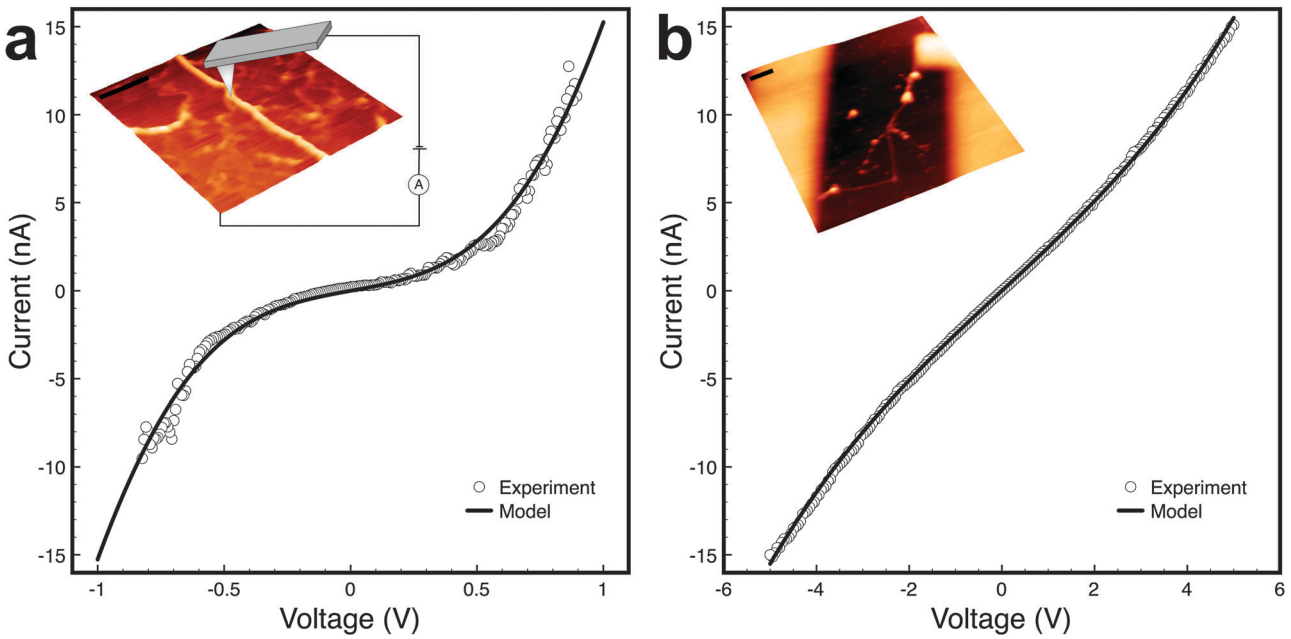


**Fig. 5** A comparison of the measured *I–V* characteristics and modeling results for two different experiments.[17,18] (a) Transverse transport across the thickness of a microbial nanowire (~10 nm), using a conductive tip as the top electrode and a supporting surface as the bottom electrode (calculation parameters: $L = 10$, $\lambda = 0.4$ eV, $\alpha = 0.3$, $C_{electrode} = 1.8 \times 10^{10}$ s$^{-1}$, $k_BT = 0.025$ eV). (b) Longitudinal transport along a microbial nanowire (2 μm) bridging two Pt electrodes (calculation parameters: $L = 2000$, $\lambda = 0.4$ eV, $\alpha = 0.015$, $C_{electrode} = 5 \times 10^{11}$ s$^{-1}$, $k_BT = 0.025$ eV). Insets show the AFM images corresponding to the measurements with 250 nm scale bars.

longitudinal transport is measured along a nanowire using two electron/ion beam deposited electrodes separated by 2 μm ($L = 2000$). The previously reported longitudinal measurements revealed linear *I–V* curves for low voltages (<1 V), but the non-linearity predicted by the model appears at higher bias, as can be seen by the experimental data reported here for the same sample (up to 5 V in Fig. 5b).

For a similar voltage range, the *I–V* measurements of the transverse and longitudinal experiments appear distinct.[17,18] However, the model is in good agreement with both measurements, as shown on Fig. 5. Both experiments were fit with a reorganization energy $\lambda$ close to 0.4 eV. While there are no experimental measurements of $\lambda$ in *Shewanella*'s cytochromes, 0.4 eV is consistent with electrochemically determined values of $\lambda$ for cytochrome *c* at electrode surfaces.[33] It should be noted that $\lambda$ measured electrochemically, with a system probing electron transfer to electrodes, is expected to be smaller than theoretical calculations in solution without electrodes, since the electrode approach decreases the outer-sphere reorganization's ($\lambda_{out}$) solvent contribution.[33,34] In addition, the experiments considered here were performed in air under ambient conditions.

Different $C_{electrode}$ and $\alpha$ parameters are expected for the two different experiments, since these parameters reflect the electronic interaction and fraction of voltage drop at the measurement contacts. In the transverse experiment, the nanowire is supported on a flat conductive surface and a metallized AFM tip is held just above the nanowire (applying a force in the nN range).[17] The resulting transport behavior was fit using $C_{electrode} = 1.8 \times 10^{10}$ s$^{-1}$. In the longitudinal experiment, Pt electrodes are directly vacuum deposited onto the nanowire surface, and this intimate electronic contact was reflected with $C_{electrode} = 5 \times 10^{11}$ s$^{-1}$. It is worth noting that both values are orders of magnitude higher than previously measured heterogeneous transfer rate constants of *Shewanella* cytochromes.[35] The reason for this wide discrepancy is not clear, but it may be attributed to the very different experimental conditions, namely the dry fixed environment of the microbial nanowire measurements, and the likelihood that the system does not adopt its native conformation under these conditions. By examining $\alpha$, we estimate that 30% of the overall voltage drop happened at the electrode-wire contact ($\alpha = 0.3$) in the transverse measurement across 10 nm, compared to 1.5% ($\alpha = 0.015$) in the measurement along a 2 μm nanowire. Indeed, it is reasonable to expect that for a longer redox chain the local voltage drop at the electrode should be smaller, relative to the total voltage, than in a shorter chain. Furthermore, we previously measured the contact resistance for a 600 nm long wire,[18] and found that the corresponding local voltage drop at the electrode is 7% of the total applied voltage, *i.e.* giving an experimentally determined $\alpha = 0.07$ for a 600 nm chain; an intermediate value between the 10 nm and 2 μm predictions, further confirming the expected trend. With the fit parameters described here (Fig. 5 and Table S1, ESI†), it is possible to calculate the voltage threshold corresponding to the saturation of transport due to the maximum overlap between the metallic Fermi function and the Gaussian redox peaks (Fig. 2 and 4). The saturation would be expected at 2.5 V and 50 V for the transverse and longitudinal measurements, respectively. These predictions are useful for designing future experiments to test and improve the model, provided that the high voltages required do not induce physical damage in the biological structures under study.

 

Next, we examine the sensitivity of the calculation to the model parameters. The assumption made that $C_{electrode}$ is smaller than $k_{hop}$ places an upper limit on the effective tunneling distance $R$. While this assumption should be easily met for most reasonable distances that sustain tunneling because of the normally very small heterogeneous transfer rates[35] (discussed above), using our higher fit values for $C_{electrode}$ ($\sim 10^{10}$ $s^{-1}$), and comparing with $k_{hop}$ (eqn (2)), suggests an upper limit $\beta R \approx 6.9$. With a typical protein decay coefficient of 1 $Å^{-1}$, this translates to an effective tunneling distance $R < 0.69$ nm (*i.e.* taking the van der Waals contact distance to be 0.35 nm, the nearest neighbor hopping distance is less than 1.04 nm). This result is consistent with the previous finding by Polizzi *et al.*,[23] and is also met by the experimentally determined heme separation distances in *Shewanella*'s multiheme cytochromes.[25] As noted above, in this regime the predicted current response follows the form of the heterogeneous electron transfer terms eqn (5) and (6), which makes the calculated *I–V* behavior very sensitive to $\lambda$ and $C_{electrode}$. Fig. S1 (ESI†) illustrates this sensitivity by showing the disagreement between model and experiment for slightly lower and higher reorganization energies, $\lambda = 0.35$ and 0.45 eV respectively, while keeping $C_{electrode}$ fixed. However, it is possible to compensate for the variation of the reorganization energy and obtain a good fit to the experimental data by tuning $C_{electrode}$ simultaneously, but only within the range 0.3 eV $< \lambda <$ 1 eV, outside which we observe disagreement between calculations and experiments in the high bias region as shown in Fig. S2 (ESI†).

Understanding the theoretical basis of extracellular charge transfer in microbial redox chains has significant implications for elucidating the natural respiratory strategies employed by important environmental bacteria. In addition, this understanding can be harnessed towards defining the limitations and realizing the untapped potential of emerging technologies (such as biofuel cells) where these bacteria are employed as electrode-bound catalysts for driving redox reactions. In light of the multistep hopping model described here (Fig. 1a), we note that efficient EET requires a favorable interaction with electrodes (described by the heterogeneous transfer rates), which may be a limiting factor in real devices, motivating us to investigate new anode materials that maximize the electronic coupling with redox molecules. Efficient EET also requires small separations between redox sites within the chain ($\sim 1$ nm);[25] a requirement that seems to be satisfied by the heme-to-heme distances of individual outer membrane cytochromes. However, this hopping picture appears to be sensitive to possible structural defects in one dimension, and microbes may address this limitation through redundancy and multiple redox chains spread over cell surfaces and extracellular appendages within three-dimensional biofilms attached to electrodes.

## 4. Conclusions

In summary, we presented a model to describe charge transfer in microbial redox chains between electrodes. After reviewing the applicability of coherent band conduction and incoherent hopping to the transport measurements of microbial nanowires, we excluded band conduction as a viable model of charge transport in these structures because the measured mobilities are far below the minimum mobility set forth by the coherent mechanism. In contrast, the incoherent hopping mechanism can account for the observed transport rates as well as the form of the current–voltage curves from transverse and longitudinal measurements of microbial nanowires. The proposed model is based on an incoherent multistep hopping mechanism between redox sites, and an interfacial treatment of the electrochemical interactions with the measurement electrodes. Using this model, we computed the occupation probability profile throughout the redox chain, which allowed the calculation of the current response to applied voltage between the electrodes. We found the results to be in good agreement with two previously reported experiments measuring transport in microbial nanowires produced by the bacterium *Shewanella oneidensis* MR-1. Furthermore, the fit parameters were consistent with the length scales and electrode contact conditions of each experiment, as well as the typical reorganization energies expected from *c* cytochromes known to be critical for this organism's extracellular charge transfer ability. Our analysis motivates further experimental and theoretical investigations into the identity and structural organization of redox components in microbial systems with significant environmental and biotechnological implications.

## Acknowledgements

We gratefully acknowledge financial support from the Air Force Office of Scientific Research (AFOSR) through YIP grant FA9550-10-1-0144 and MURI grant FA9550-06-1-0292. We also thank Greg Wanger and Tom Yuzvinsky for experimental help with nanofabrication and microscopy. Finally, we acknowledge the USC NanoBiophysics Core Facility and the USC Center for Electron Microscopy and Microanalysis for microscopy resources.

## Notes and references

1 P. Mitchell, *Nature*, 1961, **191**, 144–148.
2 H. B. Gray and J. R. Winkler, *Biochim. Biophys. Acta, Bioenerg.*, 2010, **1797**, 1563–1572.
3 K. H. Nealson, A. Belz and B. McKee, *Antonie Van Leeuwenhoek Int. J. Gen. Mol. Microbiol.*, 2002, **81**, 215–222.
4 J. A. Gralnick and D. K. Newman, *Mol. Microbiol.*, 2007, **65**, 1–11.
5 D. R. Lovley and E. J. P. Phillips, *Appl. Environ. Microbiol.*, 1988, **54**, 1472–1480.
6 C. R. Myers and K. H. Nealson, *Science*, 1988, **240**, 1319–1321.
7 H. H. Hau and J. A. Gralnick, *Annu. Rev. Microbiol.*, 2007, **61**, 237–258.
8 B. E. Logan, *Nat. Rev. Microbiol.*, 2009, **7**, 375–381.
9 D. R. Lovley, J. D. Coates, E. L. Blunt-Harris, E. J. P. Phillips and J. C. Woodward, *Nature*, 1996, **382**, 445–448.
10 D. K. Newman and R. Kolter, *Nature*, 2000, **405**, 94–97.
11 E. Marsili, D. B. Baron, I. D. Shikhare, D. Coursolle, J. A. Gralnick and D. R. Bond, *Proc. Natl. Acad. Sci. U. S. A.*, 2008, **105**, 3968–3973.
12 H. von Canstein, J. Ogawa, S. Shimizu and J. R. Lloyd, *Appl. Environ. Microbiol.*, 2008, **74**, 615–623.
13 C. R. Myers and J. M. Myers, *J. Bacteriol.*, 1992, **174**, 3429–3438.
14 T. Mehta, M. V. Coppi, S. E. Childers and D. R. Lovley, *Appl. Environ. Microbiol.*, 2005, **71**, 8634–8641.
15 G. Reguera, K. D. McCarthy, T. Mehta, J. S. Nicoll, M. T. Tuominen and D. R. Lovley, *Nature*, 2005, **435**, 1098–1101.

16 Y. A. Gorby, S. Yanina, J. S. McLean, K. M. Rosso, D. Moyles, A. Dohnalkova, T. J. Beveridge, I. S. Chang, B. H. Kim, K. S. Kim, D. E. Culley, S. B. Reed, M. F. Romine, D. A. Saffarini, E. A. Hill, L. Shi, D. A. Elias, D. W. Kennedy, G. Pinchuk, K. Watanabe, S. Ishii, B. Logan, K. H. Nealson and J. K. Fredrickson, *Proc. Natl. Acad. Sci. U. S. A.*, 2006, **103**, 11358–11363.
17 M. Y. El-Naggar, Y. A. Gorby, W. Xia and K. H. Nealson, *Biophys. J.*, 2008, **95**, L10–L12.
18 M. Y. El-Naggar, G. Wanger, K. M. Leung, T. D. Yuzvinsky, G. Southam, J. Yang, W. M. Lau, K. H. Nealson and Y. A. Gorby, *Proc. Natl. Acad. Sci. U. S. A.*, 2010, **107**, 18127–18131.
19 N. S. Malvankar, M. Vargas, K. P. Nevin, A. E. Franks, C. Leang, B. C. Kim, K. Inoue, T. Mester, S. F. Covalla, J. P. Johnson, V. M. Rotello, M. T. Tuominen and D. R. Lovley, *Nat. Nanotechnol.*, 2011, **6**, 573–579.
20 H. A. Liu, G. J. Newton, R. Nakamura, K. Hashimoto and S. Nakanishi, *Angew. Chem., Int. Ed.*, 2010, **49**, 6596–6599.
21 J. K. Fredrickson, M. F. Romine, A. S. Beliaev, J. M. Auchtung, M. E. Driscoll, T. S. Gardner, K. H. Nealson, A. L. Osterman, G. Pinchuk, J. L. Reed, D. A. Rodionov, J. L. M. Rodrigues, D. A. Saffarini, M. H. Serres, A. M. Spormann, I. B. Zhulin and J. M. Tiedje, *Nat. Rev. Microbiol.*, 2008, **6**, 592–603.
22 S. M. Strycharz-Glaven, R. M. Snider, A. Guiseppi-Elie and L. M. Tender, *Energy Environ. Sci.*, 2011, **4**, 4366–4379.
23 N. F. Polizzi, S. S. Skourtis and D. N. Beratan, *Faraday Discuss.*, 2012, **155**, 43–62.
24 C. E. D. Chidsey, *Science*, 1991, **251**, 919–922.
25 T. A. Clarke, M. J. Edwards, A. J. Gates, A. Hall, G. F. White, J. Bradley, C. L. Reardon, L. Shi, A. S. Beliaev, M. J. Marshall, Z. Wang, N. J. Watmough, J. K. Fredrickson, J. M. Zachara, J. N. Butt and D. J. Richardson, *Proc. Natl. Acad. Sci. U. S. A.*, 2011, **108**, 9384–9389.
26 H. B. Gray and J. R. Winkler, *Q. Rev. Biophys.*, 2003, **36**, 341–372.
27 F. C. Grozema and L. D. A. Siebbeles, *Int. Rev. Phys. Chem.*, 2008, **27**, 87–138.
28 S. M. Strycharz-Glaven and L. M. Tender, *Energy Environ. Sci.*, 2012, **5**, 6250–6255.
29 A. Troisi, *Org. Electron.*, 2011, **12**, 1988–1991.
30 J. C. Bellows and P. N. Prasad, *J. Chem. Phys.*, 1979, **70**, 1864–1871.
31 R. A. Marcus and N. Sutin, *Biochim. Biophys. Acta*, 1985, **811**, 265–322.
32 A. M. Kuznetsov, P. Sommerlarsen and J. Ulstrup, *Surf. Sci.*, 1992, **275**, 52–64.
33 C. A. Bortolotti, M. E. Siwko, E. Castellini, A. Ranieri, M. Sola and S. Corni, *J. Phys. Chem. Lett.*, 2011, **2**, 1761–1765.
34 S. Corni, *J. Phys. Chem. B*, 2005, **109**, 3423–3430.
35 R. S. Hartshorne, B. N. Jepson, T. A. Clarke, S. J. Field, J. Fredrickson, J. Zachara, L. Shi, J. N. Butt and D. J. Richardson, *J. Biol. Inorg. Chem.*, 2007, **12**, 1083–1094.

 